Stage-III recovery in α-iron studied by means of nuclear magnetic resonance on oriented ^{131}I nuclei

A. Metz and L. Niesen
Laboratorium voor Algemene Natuurkunde, Materials Science Centre, Groningen University, Westersingel 34, 9718 CM Groningen, The Netherlands
(Received 28 July 1988; revised manuscript received 11 October 1988)

Nuclear magnetic resonance measurements were performed on oriented ^{131}I nuclei implanted into decarburized single crystals of α-Fe. Satellite resonances, centered around 633 MHz, that are well described by an additional quadrupole interaction with a $\langle 111 \rangle$ symmetry appeared both after room-temperature implantation and after low-temperature Frenkel pair production followed by annealing at a temperature corresponding with recovery stage III. The results from a defect-antidefect reaction with mobile stage-I defects strongly indicate that these satellite resonances are caused by trapping of mobile vacancies. Implantation at 20 K and a comparatively low dose resulted in a high-field fraction of 0.9, which is much higher than usually obtained after room-temperature implantation. Two newly discovered satellite patterns, centered around 647 and 660 MHz, are attributed to additional trapping of oxygen and hydrogen impurities, respectively.

I. INTRODUCTION

Stage-III recovery in α-Fe is the subject of a long-standing controversy. Whereas state I_E is attributed to the long-range migration of a point defect of interstitial type, two different defect types have been proposed for stage III, which occurs in α-Fe around 220 K. Recent experimental results obtained by microscopic methods, such as positron annihilation[1] and muon spin rotation,[2] provide evidence in favor of the so-called one-interstitial model (OIM). According to this model vacancies become mobile in stage III. Other experimental results, as obtained by means of high-voltage electron microscopy[3] and by internal friction[4] and magnetic after-effect[5] measurements, are interpreted in terms of the two-interstitial model (TIM). According to the TIM a second type of interstitial becomes mobile in stage III. A recent review of the recovery behavior of α-Fe is given by Takaki *et al.*[6]

Past attempts to attack this problem with hyperfine interaction techniques such as Mössbauer spectroscopy[7] or perturbed angular correlations,[8,9] suffered from their inability to resolve the details of the defect-induced quadrupole interaction in the presence of a strong magnetic interaction. We therefore decided to study stage-III recovery in α-Fe by means of nuclear magnetic resonance on oriented nuclei (NMRON). This technique is very sensitive to the hyperfine interaction of a radioactive impurity with its nearby surroundings. The principle of the method is the destruction, by an applied radio frequency (rf) field, of the anisotropy of the radiation that is emitted in the radioactive decay of the probe atom. The anisotropy of the radiation is achieved by cooling the sample in a static magnetic field to temperatures in the millikelvin region, thus orienting the nuclear spins parallel to the magnetic field. Details of the method can be found in Ref. 10 and references cited therein.

Visser *et al.*[11] were the first to observe defect association with NMRON, after room-temperature (RT) implantation of ^{131}I into single crystals of α-Fe. They observed two different hyperfine fields, a high field of 114.67(1) T and a lower field of 105.97(5) T. Additionally, an electric field gradient in the $\langle 111 \rangle$ direction was observed for the lower-field site, which was ascribed to a nearest-neighbor monovacancy.

The work presented here is a continuation of the work of Visser *et al.*[11] In Sec. IV A we report on uncorrelated defect trapping at ^{131}I in recovery stage III after the sample had been irradiated with light energetic particles at low temperatures. In Sec. IV B we investigate the effect of implantation of ^{131}I at 20 K in order to exclude the influence of thermally activated vacancy migration on the formation of the ^{131}I-defect complex. Section IV C is devoted to the interaction of the observed ^{131}I-defect complex with mobile interstitials below stage III. Impurity-associated resonances are reported in Sec. IV D.

A preliminary account of this work has been published in Ref. 12.

II. DEFECT-ASSOCIATED RESONANCES

Visser *et al.*[11] observed defect-associated resonances centered around 633 MHz, the splitting of which depends on the direction of magnetization with respect to the crystallographic axes. They described the interaction of the ^{131}I-defect complex by the following Hamiltonian:

$$H = -g_N\mu_N(\mathbf{B}_{\rm HF}+\mathbf{B}_{\rm ext}-\mu_0 N\mathbf{M})\cdot\mathbf{I}-g_N\mu_N\mathbf{B}_{\rm dip}\cdot\mathbf{I} + \frac{e^2qQ}{4I(2I-1)}[3I_{z'}^2-\mathbf{I}\cdot\mathbf{I}+\eta(I_{x'}^2-I_{y'}^2)] \quad (1)$$

Here, μ_N is the nuclear magneton, $g_N=0.7834(3)$ is the nuclear g-factor, and $Q=-0.40(1)$ b is the nuclear quadrupole moment of ^{131}I.[13] $\mathbf{B}_{\rm HF}$, $\mathbf{B}_{\rm ext}$, and $\mu_0 N\mathbf{M}$ are the magnetic hyperfine field, the external field, and the

demagnetizing field, respectively, the last of which depends on the shape of the sample through the tensor N. Here, these fields are assumed to be parallel and they define the z axis of the coordinate system. The other terms in the Hamiltonian express the interactions that break the axial symmetry and, therefore, are responsible for the observed splitting of the resonance lines. These are the dipolar field, $\mathbf{B}_{\rm dip}$, and the electric-field-gradient (EFG) tensor with largest component eq and asymmetry parameter η, caused by the defect. The principal axes system of the EFG is marked by primes.

Because the symmetry-breaking terms are relatively small, we choose as a basis the axially symmetrical eigenfunctions of I_z, the eigenvalues of which are the magnetic quantum numbers m, and neglect nondiagonal matrix elements. This results in the following approximate expression for the resonance frequencies:[14]

$$h\nu_{m,m-1}=g_N\mu_N(B_{\rm HF}+B_{\rm ext}-\mu_0 NM)+g_N\mu_N B_{\rm dip}(\alpha,\beta) - \frac{3e^2qQ}{4I(2I-1)}(2m-1)[P_2(\cos\beta) + \tfrac{1}{2}\eta\sin^2\beta\cos2\alpha] . \quad (2)$$

Here, the Euler angles α and β define the orientation of the principal axis system of the EFG tensor with respect to the crystallographic axes. In general, the resonance for each particular orientation (α,β) will split into $2I=7$ components. If these are not resolved, as is the case in the present work, only one line is observed for each orientation, at a frequency which is mainly determined by the transition between the two lowest nuclear sublevels. This is so because only these sublevels are significantly populated at the temperatures used.

Visser *et al.*[11] concluded that the ^{131}I-defect complex possesses a $\langle 111\rangle$ symmetry axis, from the following arguments. In the case $\mathbf{B}\|\langle 100\rangle$, a single resonance line was observed. This is only possible if the orientation of the EFG tensor with respect to $\mathbf{B}$, is equal for the three equivalent orientations of $\mathbf{B}$. The EFG main axis must therefore be oriented along a $\langle 111\rangle$ crystallographic axis. Moreover η has to be small, because even for an EFG with a $\langle 111\rangle$ main axis, a nonzero η would cause splitting of the resonance line. Taking into account the observed linewidth of 5 MHz for the $\langle 100\rangle$ crystal, we obtain $\eta\leq 0.3$ on the basis of Eq. (2). A general expression for the angular dependence of the dipole field $B_{\rm dip}(\alpha,\beta)$ cannot be given without detailed knowledge of the structure of the defect complex. Visser *et al.*,[11] assumed that the defect is a monovacancy on a nearest-neighbor position, and this assumption is supported by our results. In this case the dipolar field may be evaluated by removing a single iron moment from a nearest-neighbor position. This results in an additional term $B_{\rm dip}\cdot P_2(\cos\theta)$, where θ is the angle between the z axis and the z' axis. For this particular case the resonance frequency may be approximated as

$$\nu_{I,I-1}=\nu_0+\nu_1 P_2(\cos\theta) , \quad (3a)$$

where

$$\nu_0=\frac{g_N\mu_N}{h}(B_{\rm HF}+B_{\rm ext}-\mu_0 NM) , \quad (3b)$$

$$\nu_1=\frac{1}{h}\left[g_N\mu_N B_{\rm dip}-\frac{3e^2qQ}{4I}\right] . \quad (3c)$$

Using values of $B_{\rm HF}=106.1$ T, $B_{\rm dip}=-0.267$ T, and $eq=1.05\times10^{22}$ V/m^2, Visser *et al.* obtained good fits to the majority of the observed resonance frequencies.

It should be noted, however, that although the $\langle 111\rangle$ symmetry of the ^{131}I-defect complex is quite well established, the value of eq is not. The reason for this is that the value of the dipolar field $B_{\rm dip}$ cannot be determined from the experimental results. In fact any two values of eq (in V/m^2) and $B_{\rm dip}$ (in T) that satisfy the relation

$$eq=+0.98\times10^{22}(1.0-0.28\times B_{\rm dip}) \quad (4)$$

would fit the experimental data quite well as long as the relative contributions from the EFG and the dipolar field to the total hyperfine interaction are small. Although, in principle, the observation of the fine structure of the resonance lines could solve this problem, the available experimental data do not allow us to make any definite conclusion.

III. EXPERIMENTAL PROCEDURE

The single crystals of α-Fe used in the present experiments were obtained from the Max Planck Institut für Metallforschung in Stuttgart, West Germany. There the crystals were grown with the strain anneal technique from Johnson Matthey material, whereafter they were treated with hydrogen to minimize the carbon content, while probably also reducing the nitrogen concentration. The final resistance ratio, $\Gamma=580$, is mainly due to metallic impurities. The carbon and oxygen contents were determined by means of charged particle activation analysis at the Institut für Kernphysik of the University of Frankfurt, West Germany. The carbon concentration was found to be less than 0.4 ppm; the oxygen concentration was less than 2.5 ppm. The nitrogen concentration could not be determined accurately. The samples were cut into rectangular pieces, the dimensions of which are given in Table I. The orientations of the long axes of the samples were determined by means of x-ray diffraction, and are given in Table I in terms of the polar angles (θ,ϕ) with respect to the main crystallographic axes. We will distinguish the two samples by their approximate orientations $\langle 651\rangle$ and $\langle 610\rangle$.

The samples were soldered with indium on copper sample holders, which could be screwed into the various experimental units that we used. Before implantation, the crystal surfaces were mechanically polished and electrochemically etched, using a mixture of 5 ml perchloric acid (70%) and 100 ml acetic acid (100%). The etching was done after soldering the samples on the sample holders in order to avoid possible contamination of the implanted layer with indium, except in the case that the sample had to be annealed above the melting point of indium (430 K).

TABLE I. Specifications of the single crystals.

Approximate orientation	θ (deg)	ϕ (deg)	Dimensions (mm)	Demagnetizing factors (N_x, N_y, N_z)
⟨651⟩	38(1)	11(1)	0.9×3.4×14.0	0.776, 0.199, 0.026
⟨610⟩	10(1)	0(1)	1.3×3.5×13.6	0.708, 0.254, 0.037

^{131}I was implanted into the crystals, both at room temperature and at 20 K. During the low-temperature implantations, the sample was cooled with a closed-cycle helium refrigerator. Irradiations with energetic particles were performed with the same refrigerator connected to a beam line of the Groningen van de Graaff accelerator. The samples were transferred from the closed-cycle refrigerator to the dilution refrigerator used for the NMRON measurements in a portable liquid-nitrogen cryostat in which they could be kept at 80 K. They were introduced into the dilution refrigerator by means of a top-loading system. During the transfer the sample warmed up to at most 100 K. After this the base temperature of the dilution refrigerator (14 mK), could be reached within a few hours.

The temperature of the mixing chamber was monitored with a ^{60}CoCo nuclear orientation thermometer. Both samples were magnetized along their long axes in order to minimize the external field necessary to magnetize the samples.

The radiative destruction of anisotropy was observed on the 364-keV transition in the decay of ^{131}I with a 63×63 mm^2 NaI(Tl) detector. The gain of the detection system was stabilized by means of count-rate difference feedback to the detector high voltage.

The intensity $W(\theta)$ of the emitted radiation as a function of the angle θ between the applied magnetic field and the direction of observation can be described by

$$W(\theta)=\sum_{k=0,2,4} U_k F_k Q_k B_k P_k(\cos\theta) \ . \tag{5}$$

Here, U_k takes into account the deorientation of the nuclear spins due to unobserved transitions, F_k describes the angular distribution of the observed γ radiation, B_k describes the degree of orientation of the parent level, and Q_k is a correction factor that accounts for the finite solid angle subtended by the detector. Koene and Postma[15] have measured the following values: $U_2F_2=0.213(7)$, $U_4F_4=0.41(7)$. At high temperatures, $W(\theta)=1$, independent of θ. At sufficiently low temperatures, the nuclear spins become oriented and $W(\theta)$ will be different from 1. In the following we will use the term anisotropy for $W(0)-1$.

NMRON measurements were performed by sweeping the rf up and down over the frequency region of interest, collecting counts at each frequency point during 20 s, while switching the frequency modulation (FM) alternatively on and off. After switching the modulation off, data acquisition was interrupted for 1 s to allow for spin-lattice relaxation. Because it was impossible to match the rf-coil impedance perfectly to that of the transmission line over the full frequency interval of interest, the measurements suffered slightly from variations in rf power, and thus also from changes in the anisotropy as a function of time. These changes led to a small difference in anisotropy between FM-on and FM-off counting periods. To correct for this undesired effect, the FM-off count rates were calculated by linear interpolation between the two neighboring FM-off count rates of a FM-on frequency point. This procedure results in a satisfactory flat background, obviously because the changes in anisotropy are governed by the slow thermal response of the dilution refrigerator.

In the figures in Sec. IV we show, as a function of the frequency ν, the destruction of anisotropy $D(\nu)$, defined as

$$D(\nu)=\frac{N_{\text{FM-off}}(\nu)-N_{\text{FM-on}}(\nu)}{N_{\text{FM-off}}(\nu)-N_{\text{warm}}} \ . \tag{6}$$

Here, N_{warm} is the count rate at a temperature where the anisotropy is zero. In this way the effects of varying rf power are largely eliminated.

The total area of a resonance peak divided by the modulation width, i.e., the integrated destruction of anisotropy $[D^I(\nu)]$, measures the relative fraction of the anisotropy destroyed in this resonance and is related to the corresponding site population f_i of the implanted atoms as follows:

$$f_i=\frac{D_i^I(\nu) f_{N0,i}}{P_{\text{rf},i}} \ , \tag{7a}$$

with

$$f_{N0,i}=\frac{[W(0)-1]_{\text{obs}}}{[W_i(0)-1]_{\text{calc}}} \ . \tag{7b}$$

Here,

$$[W(0)-1]_{\text{obs}}=N_{\text{FM-off}}(\nu)/N_{\text{warm}}-1$$

is the total observed anisotropy, $[W_i(0)-1]_{\text{calc}}$ is the calculated anisotropy for nuclei on site i, and P_{rf} is the rf-saturation factor. $[W_i(0)-1]_{\text{calc}}$ is calculated using the known hyperfine field and the temperature of the mixing chamber. The relative difference between the calculated anisotropies for the defect associated field and the substitutional field amounts to at most 5% and was neglected because the uncertainties in P_{rf} are probably larger. Therefore we calculated only f_{NO} (where NO stands for nuclear orientation), which refers to the substitutional site. The calculated value may be in error because of incomplete magnetization of the samples or a temperature gradient between the mixing chamber and the sample.

Ideally, the rf saturation factor equals 1. However, in our experiments this value was never obtained. Although full rf saturation can be attained by increasing the rf power, this will excessively heat the sample, thereby reducing the anisotropy and, thus, the NMR signal.

It should be noted that the IDA for the quadrupole-split defect lines is, in principle, not equal to the IDA for a purely magnetic interaction, because in the latter case the population of all nuclear sublevels tends to become equal. Calculations that will be discussed in Sec. IV show that there is also a contribution to the IDA from the NMR transition between the second and the third energy level ($\nu_{I-1,I-2}$). As a result the total IDA for full rf saturation is about 120%, whereas for a purely magnetic interaction it would be 100%. However, in most cases the splitting between $\nu_{I,I-1}$ and $\nu_{I-1,I-2}$ is smaller than the modulation width, and then the total IDA is close to 100%.

In the tables in Sec. IV we will present tentative values for the site populations f_i. These are subject to uncertainties in the common factors $[W_i(0)-1]_{\text{calc}}$ and P_{rf}, as explained above. These uncertainties, however, vary only a little over the different measurements, because we took care to keep the magnetizing field and the rf power constant. Although the reported values of f_i are not absolute values, they allow us to determine changes in the site populations.

IV. RESULTS

In Fig. 1 we show the experimental line shapes of the defect-associated resonances for the ⟨610⟩ and the ⟨651⟩ crystals. The corresponding histograms represent line shapes that were calculated as follows. Using the values of Visser *et al.* (Ref. 11), $B_{\text{HF}}=106.1T$, $B_{\text{dip}}=-0.267T$, and $eq=1.05\times10^{22}$ V/m^2, and diagonalizing the full Hamiltonian, $D(\nu)$ was calculated for each allowed transition between the nuclear sublevels. We applied the so-called fast-relaxation limit, in which it is assumed that the nonresonated levels are occupied according to a Boltzmann distribution with respect to the resonated levels.[16] The effect of the inhomogeneous linewidth was neglected because it would complicate the calculation considerably. The effect of frequency modulation was taken into account by assuming that all spin transitions within the modulation width are actually stimulated. In order to obtain a close agreement with the experimental resonance frequencies, while keeping eq and B_{dip} equal to the values quoted above, deviations in the crystal orientations of at most 7° had to be assumed. Such a misorientation may have occurred during the soldering of the crystals.

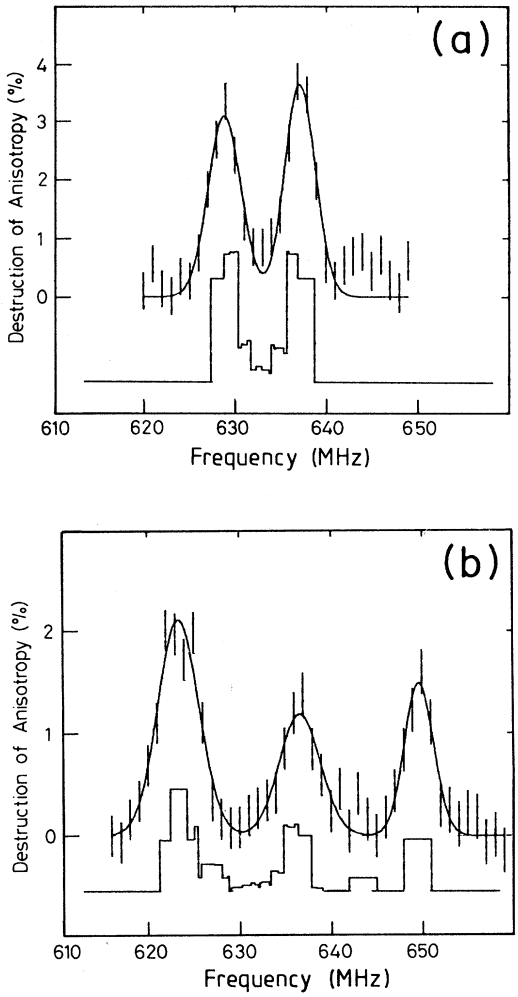

FIG. 1. (a) Defect-associated resonances for ⟨610⟩ orientation. (b) Defect-associated resonances for ⟨651⟩ orientation. Error bars: experimental data. Histogram: calculated line shape for 3.0 MHz modulation width and zero inhomogeneous linewidth.

A. Uncorrelated defect trapping

The purpose of this experiment was to determine whether the ^{131}I-defect complex found after RT implantation is also formed after irradiation with light energetic particles, and in which recovery stage it is formed.

The ⟨651⟩ crystal was implanted at RT with 110-keV ^{131}I ions to a source strength of 8.3 MBq. The dose was 2×10^{13} ^{131}I/cm^2 corresponding with a maximum impurity concentration of 25 ppm at a depth of 20 nm. Here, and in the following experiments, the total implanted dose could not be determined accurately, but is estimated to be 2 to 3 times the radioactive dose. The sample was annealed at 575 K for 30 min and subsequently irradiated at 40 K with 2 MeV protons to a dose of 5×10^{16} H$^+$/cm^2. The resulting Frenkel pair concentration, derived from the tables of Jung,[17] is approximately 700 ppm. At this defect concentration, stage III is expected to have its peak temperature around 200 K (Ref. 6). As mentioned before, the sample warmed up to 100 K during transfer to the dilution refrigerator. Final annealings for 30 min were performed at 185 K and 240 K. All NMRON measurements were performed at an external field of 120 mT, where the magnetization is almost complete. The modulation width was 3.0 MHz for the defect-associated lines and 0.5 MHz for the substitutional

resonances. Close to 620 MHz the measurements are unreliable because the rf power varied strongly with frequency. This power resonance was removed after this experiment. The temperature of the mixing chamber varied between 15 and 25 mK. The spectra recorded for the defect-associated lines are shown in Fig. 2 and those for the substitutional resonances in Fig. 3. After RT implantation we found $f_{N0}=0.5(1)$, which is in reasonable agreement with earlier results.[11,15,18] This value did not change within experimental accuracy during the various treatments of the sample.

The frequencies of the defect-associated resonances were determined by fitting each line with a single Gaussian. For the determination of the IDA of these resonances we relied on a simple summation over the scanned frequency region, because we could not always obtain a good fit with Gaussians. This procedure resulted in an IDA of about 3%, even when no defect lines were observed, possibly because the time dependence of the anisotropy was not completely accounted for in the interpolation procedure. For the substitutional resonances we used a two-component Gaussian, which gave satisfactory results for the majority of the measurements. The broad component is assumed to be caused by lattice damage outside the nearest-neighbor shell. The width of this component was found to increase with increasing damage concentration. The resulting values of frequencies and site populations are summarized in Table II and Table III, respectively. From the as-implanted spectrum we calculate the center frequency of the defect-associated resonances as 632.23(33) MHz, and for the substitutional resonance we obtain 683.90(2) MHz. After correcting for the external magnetic field, and assuming an axially symmetric EFG, these values yield the following magnetic hyperfine fields: 105.96(6) T and 114.62(1) T. They are in good agreement with earlier determinations.[11]

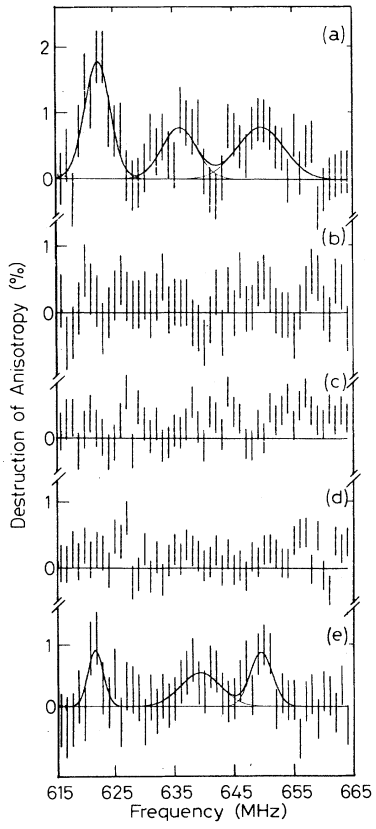

FIG. 2. Defect-associated resonances for uncorrelated trapping experiment, measured with a modulation width of 3.0 MHz. (a) as implanted at RT; (b) annealed at 575 K; (c) irradiated with 5×10^{16} H^+/cm^2 at 40 K, and subsequently warmed up to 100 K; (d) annealed at 180 K; and (e) annealed at 240 K.

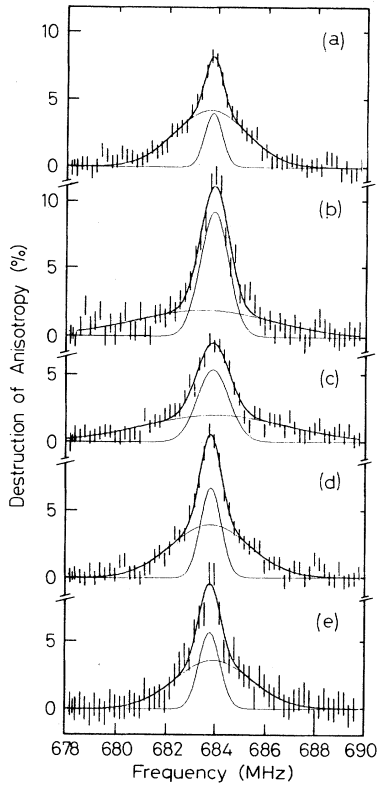

FIG. 3. Substitutional resonances for defect-trapping experiment, measured with a modulation width of 0.5 Mhz. Parts (a)–(e) are as for Fig. 2.

After annealing at 575 K, the implantation damage near the probe is largely reduced. This can be inferred from the disappearance of the defect-associated resonances, and from the increase of the narrow component and the decrease of the broad component of the substitutional resonances. We did not anneal at a higher temperature, because from the work of Visser[19] this is known to result in a reduction of the substitutional fraction. After irradiation at 40 K, the increased damage concentration showed up as a broadening of the substitutional line. After annealing at 180 K, the substitutional line had become narrower, indicating the partial recovery of radiation damage, probably as a result of migrating stage-I defects. Only after annealing at 240 K, above the expected temperature for stage III, did we observe the defect-associated resonances again, while at the same time the

TABLE II. Frequency data for uncorrelated defect trapping experiment (Sec. IV A). All values are in MHz.

Substitutional line							
Narrow component		Broad component			Defect lines		
Frequency	FWHM	Frequency	FWHM	Frequency	Frequency	Frequency	Sample treatment
683.86(4)	0.8(1)	683.74(7)	3.4(2)	622.1(4)	635.8(8)	649.5(9)	Implanted RT
683.96(3)	1.3(1)	683.6(3)	6.4(10)				Annealed 575 K
683.94(4)	1.5(1)	684.0(2)	6.7(7)				Irradiated 40 K[b]
683.85(3)	1.0(1)	683.8(1)	3.7(3)				Annealed 180 K
683.80(1)	1.0[a]	683.9(1)	3.6(4)	621.8(6)	639.3(13)	649.5(6)	Annealed 240 K

[a]FWHM fixed.
[b]Warmed up to 100 K after irradiation.

narrow component of the substitutional fraction markedly decreased. The lowest and highest resonance frequency were found at the same frequencies as after implantation, whereas the intermediate frequency had slightly shifted. This shift may be attributed to a small change of the orientation of the crystal, that had to be soldered again after annealing at 575 K. The $D^I(\nu)$ derived from Fig. 2(e) amounts to 4.6%. Although the statistics are not very good, the main features of this spectrum agree well with the calculated resonance pattern.

We conclude that the point defect that becomes mobile in α-Fe in stage III is the same defect that gets trapped at an iodine atom during implantation at RT and causes a hyperfine interaction with a $\langle 111 \rangle$ axis of symmetry.

B. Low-temperature implantation

This experiment was carried out in order to study to what extent the implanted ^{131}I atoms associate with the stage-III defect if the implantation is carried out at a temperature at which this defect is not mobile.

The $\langle 651 \rangle$ crystal was implanted at 20 K with 110 keV ^{131}I ions to a source strength of 5.0 MBq. The dose was 1.3×10^{13} ^{131}I/cm^2, corresponding with a maximum iodine concentration of 15 ppm at a depth of 20 nm. During transfer to the dilution refrigerator the sample warmed up to 100 K. Further annealings for 30 min were carried out at 130, 185, and 225 K. NMRON spectra were recorded applying an external field of 120 mT, and a modulation width of 3.0 MHz for the defect-associated resonances and 1.6 MHz for the substitutional resonance. During these measurements the temperature of the sample varied between 18 and 25 mK. The rf saturation was by no means complete as was shown by the fact that a decrease of the modulation width from 1.6 to 0.5 MHz caused a 40% increase of the $D^I(\nu)$. We conclude that $P_{rf} \leq 0.7$ and used the upper limit in calculating the site populations reported in Table V.

The spectra for the defect-associated resonances are shown in Fig. 4 and those for the substitutional resonance in Fig. 5. Data for the frequencies are summarized in Table IV, and those for the site populations in Table V. The center frequencies of defect-associated and substitutional lines were 633.08(10) MHz and 684.02(6) MHz, respectively. After correction for the external magnetic field these frequencies lead to the following values of the hyperfine fields: 106.10(2) T and 114.64(1) T. The substitutional field agrees with the value given in Sec. IV A, whereas the defect field is slightly larger than observed before.

The most striking feature of the spectra observed after low-temperature implantation is the large width of the substitutional resonance, indicating that a lot of damage exists in the nearby surroundings of the probe atom. Also the value $f_{NO}=0.9(1)$ is much higher than after RT implantation. It should be noted that this may be the result of the lower dose used in the present experiment. In an earlier experiment we implanted 2.5×10^{13} ^{131}I/cm^2 at 20 K and found $f_{NO}=0.6(1)$.

During annealing through stage I the substitutional resonance narrowed considerably, indicating a recom-

TABLE III. Site population data for uncorrelated defect trapping experiment (Sec. IV A). For P_{rf} a value of 0.7 was assumed.

Substitutional line						
Narrow component	Broad component	Total	Defect lines	All lines	f_{NO}	Sample treatment
0.05(1)	0.23(5)	0.28(6)	0.053(13)	0.33(7)	0.5(1)	Implanted RT
0.12(3)	0.21(5)	0.33(7)	0.036(8)	0.36(7)	0.5(1)	Annealed 400 K
0.19(4)	0.19(5)	0.37(7)	0.014(7)[a]	0.39(8)	0.5(1)	Annealed 575 K
0.12(3)	0.20(5)	0.32(7)	0.025(7)[a]	0.35(7)	0.5(1)	Irradiated 40 K[b]
0.10(2)	0.24(5)	0.34(7)	0.020(6)[a]	0.35(7)	0.5(1)	Annealed 180 K
0.04(1)	0.25(5)	0.29(6)	0.032(8)	0.32(7)	0.5(1)	Annealed 240 K

[a]No resonance lines observed.
[b]Warmed up to 100 K after irradiation.

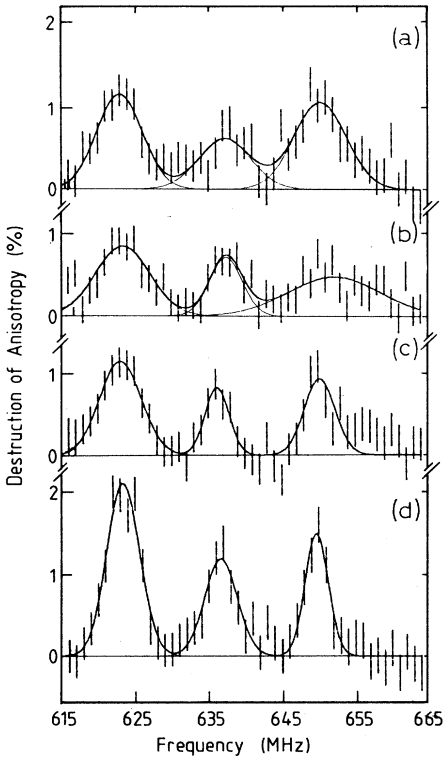

FIG. 4. Defect-associated resonances for low-temperature implantation experiment, measured with a modulation width of 3.0 MHz. (a) as implanted at 20 K, and subsequently warmed up to 100 K; (b) annealed at 130 K; (c) annealed at 185 K; and (d) annealed at 225 K.

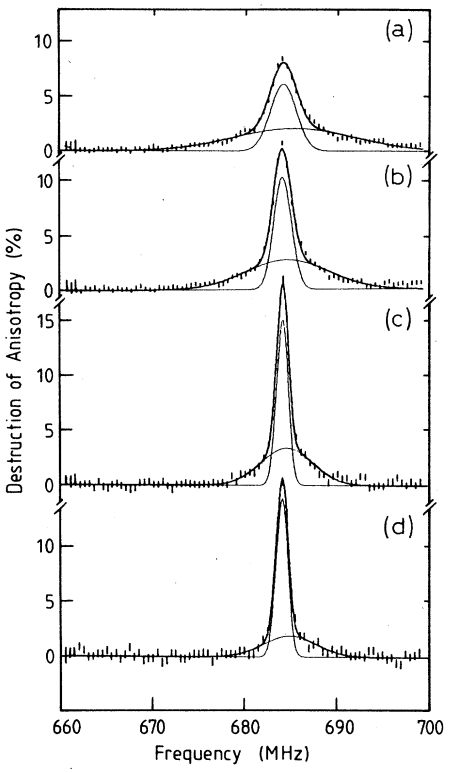

FIG. 5. Substitutional resonances for low-temperature implantation experiment, measured with a modulation width of 1.6 MHz. Parts (a)–(d) are as for Fig. 4.

bination of defects. At the same time we observed a reduction of the defect fraction. Annealing at 185 K caused a further narrowing of the broad component of the substitutional resonance.

During annealing in stage III, the defect fraction increased, while the broad component of the substitutional fraction decreased. Also the linewidth of the defect-associated resonances became smaller. This indicates correlated trapping: Point defects that were a few atomic distances from the probe atom are trapped in the nearest-neighbor shell. This process occurs at about the same temperature at which free migration of the stage-III defect was observed (cf. Sec. IV A).

C. Postirradiation below stage III

In this experiment we studied the interaction of mobile stage-I defects with trapped stage-III defects. The ⟨610⟩ crystal was implanted at RT with 110 keV ^{131}I ions to a source strength of 6.1 MBq. The dose was 1.6×10^{13} ^{131}I/cm^2, corresponding to a maximum iodine concentration of 20 ppm at a depth of 20 nm. The sample was annealed at 575 K, in order to reduce implantation damage, and subsequently irradiated at 225 K with 2 MeV He^+ ions to a dose of 3×10^{15} atoms/cm^2. During transfer to the dilution refrigerator, unintended warming up to RT took place, whereafter the first NMRON measurements were carried out. Subsequently the sample was irradiated twice at 150 K with doses of 3×10^{15} He^+/cm^2 and

TABLE IV. Frequency data for low-temperature implantation experiment (Sec. IV B). All values are in MHz.

Substitutional line				Defect lines			
Narrow component		Broad component					
Frequency	(FWHM)	Frequency	(FWHM)	Frequency	Frequency	Frequency	Sample treatment
684.12(3)	3.4(1)	685.3(2)	15.4(7)	623.0(3)	637.3(7)	650.3(4)	Implanted 20 K[a]
683.99(2)	2.3(1)	684.5(2)	10.6(5)	623.4(4)	637.5(4)	650.3(4)	Annealed 130 K
683.97(1)	1.5(1)	684.5(1)	6.6(4)	623.1(3)	636.2(3)	650.2(3)	Annealed 185 K
684.02(2)	1.5(1)	684.9(3)	6.7(7)	623.4(2)	636.6(3)	649.7(2)	Annealed 225 K

[a]Warmed up to 100 K after implantation.

TABLE V. Site population data for low-temperature implantation experiment (Sec. IV B). For P_{rf} we assumed a value of 0.7 (see text).

Substitutional line						
Narrow component	Broad component	Total	Defect lines	All lines	f_{NO}	Sample treatment
0.17(2)	0.27(3)	0.44(4)	0.104(13)	0.54(6)	0.9(1)	Implanted 20 K[a]
0.19(2)	0.27(3)	0.46(4)	0.083(10)	0.54(6)	0.9(1)	Annealed 130 K
0.19(2)	0.21(3)	0.40(4)	0.074(10)	0.47(6)	0.9(1)	Annealed 185 K
0.19(2)	0.11(2)	0.30(4)	0.102(13)	0.42(5)	0.9(1)	Annealed 225 K

[a]Warmed up to 100 K after implantation.

5×10^{15} He^+/cm^2. Next, it was annealed at 225 K, and finally irradiated at 40 K with 8×10^{15} He^+/cm^2. The particle energy was 2 MeV in all cases.

NMRON measurements were carried out, while an external field of 110 mT was applied, at which field the magnetization was nearly complete. During the measurements the temperature of the sample varied between 22 and 30 mK. The spectra for defect-associated and substitutional resonances were recorded with a modulation width of 3.0 and 0.5 MHz, respectively, and are shown in Figs. 6 and 7. Increasing the modulation width for the substitutional line from 0.5 5 to 3.0 MHz led to a 15% decrease of the $D^1(\nu)$, thus showing that the rf saturation was incomplete. We tentatively assumed $P_{rf}=0.85$. The data for the frequencies are summarized in Table VI and those for the site populations in Table VII. The center frequencies for defect and substitutional resonances were found to be 632.63(10) and 683.64(1) MHz, respectively.

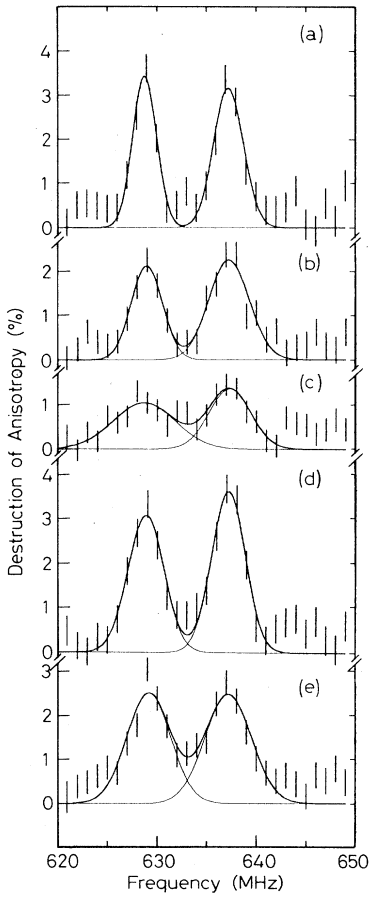

FIG. 6. Defect-associated resonances for postirradiation experiment, measured with a modulation width of 3.0 MHz. (a) irradiated with 3×10^{15} He^+/cm^2 at 225 K, and subsequently warmed up to 300 K; (b) postirradiated with 3×10^{15} He^+/cm^2 at 150 K; (c) postirradiated with 5×10^{15} He^+/cm^2 at 150 K; (d) annealed at 225 K; and (e) postirradiated with 8×10^{15} He^+/cm^2 at 40 K, and subsequently warmed up to 100 K.

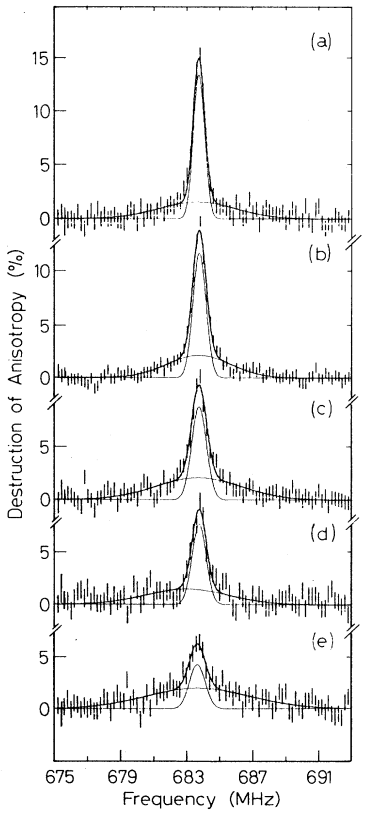

FIG. 7. Substitutional resonances for postirradiation experiment, measured with a modulation width of 0.5 MHz. Parts (a)–(e) are as for Fig. 6.

TABLE VI. Frequency data for postirradiation experiment (Sec. IV C). All values are in MHz.

Substitutional line						
Narrow component		Broad component		Defect lines		
Frequency	(FWHM)	Frequency	(FWHM)	Frequency	Frequency	Sample treatment
683.73(2)	0.8(1)	683.6(3)	5.5 (9)	628.8(3)	637.3(2)	Irradiated 225 K
683.74(1)	0.9(1)	683.7(2)	4.5 (5)	628.9(2)	637.2(2)	Irradiated 150 K
683.73(2)	1.1(1)	683.7(2)	6.1 (7)	628.7(7)	637.3(5)	Irradiated 150 K
683.75(3)	1.0(1)	683.0(5)	6.0[a]	628.9(2)	637.2(2)	Annealed 225 K
683.66(6)	1.1(2)	683.7(3)	7.4 (9)	629.2(3)	637.2(3)	Irradiated 40 K[b]

[a]FWHM fixed.
[b]Warmed up to 100 K after irradiation.

After correcting for the external magnetic field these values yield the following magnetic hyperfine fields: 106.06(2) T and 114.61 T. Both values are in agreement with the values found for the ⟨651⟩ crystal in Secs. IV A and IV B.

As a result of the postirradiations, the broad component of the substitutional resonances increased at the cost of the narrow component. The defect fractions did not change within experimental error, but the substitutional fraction clearly increased with increasing dose.

Upon annealing through stage III the substitutional fraction decreased while the defect fraction increased, thus clearly showing the trapping of the stage-III defect. Meyer and Turos[20] have shown that the substitutional fraction may increase by recoil dissolution of defects rather than by defect-antidefect reactions. Therefore, we performed a final postirradiation at a temperature below stage I with the same total dose as used in the preceding two postirradiations. This final irradiation only affected the width of the resonance lines but did not significantly change the substitutional fraction, nor the defect fraction. We conclude that the observed changes in site population after postirradiation at 150 K were mainly caused by mobile stage-I defects.

D. Influence of impurity atoms

In addition to the defect-associated resonance patterns that were reported on in the preceding sections, we found a number of resonances that cannot be described in terms of the patterns given by Visser *et al.*[11] Our first attempts to reproduce their data were carried out on single crystals of 99.9% purity from the Materials Research Corporation. After room-temperature implantation of ^{131}I we did a number of unsuccessful scans around the expected resonance frequency of 633 MHz. Eventually we found a single resonance line at 647.1(7) MHz, applying an external field $\mathbf{B}\|\langle 100\rangle$. This quite unexpected result cannot yet be fully explained, although it is likely that the resonance is caused by association of a light impurity with the earlier found ^{131}I-defect complex. The absence of other resonance lines indicates that this ^{131}I-defect-impurity complex also causes a hyperfine interaction with a ⟨111⟩ axis of symmetry. Charged particle activation analysis revealed that this sample contained carbon to a concentration of 1 ppm, whereas the oxygen concentration was 35 ppm. It is clear, therefore, that the new resonance line was not caused by carbon, whereas oxygen is likely to be the associated impurity.

Still another resonance was found after proton irradiation above stage III. The ⟨610⟩ crystal, that had been implanted at RT, was annealed at 575 K and subsequently irradiated at 225 K to a dose of 5×10^{16} H^+/cm^2. The particle energy was 1 MeV, and the corresponding proton range about 6 μm. Instead of the usual defect lines at 629 and 637 MHz, two new resonances with equal IDA were found at 657.0(6) and 663.6(6). The NMRON spectrum for this measurement, which was carried out with a modulation width of 3.0 MHz, is shown in Fig. 8. We suppose that these lines are caused by hydrogen trapped at the stage-III defect, because H is very mobile in Fe. Typical values for the diffusion of H in Fe are[21] $D_0=7.5\times10^{-4}$ cm^2/s and $U=0.088$ eV, implying long-range migration even at 225 K. Although the symmetry

TABLE VII. Site population data for postirradiation experiment (Sec. IV C). For P_{rf} a value of 0.85 was assumed (see text).

Substitutional line						
Narrow component	Broad component	Total	Defect lines	All lines	f_{NO}	Sample treatment
0.12(2)	0.10(2)	0.23(3)	0.050(6)	0.28(4)	0.45(5)	Irradiated 225 K
0.14(2)	0.12(2)	0.26(3)	0.046(6)	0.30(3)	0.49(5)	Irradiated 150 K
0.13(2)	0.20(3)	0.33(4)	0.042(5)	0.37(4)	0.58(5)	Irradiated 150 K
0.10(1)	0.16(3)[a]	0.26(3)	0.074(8)	0.33(4)	0.54(5)	Annealed 225 K
0.06(1)	0.18(3)	0.24(3)	0.065(8)	0.31(4)	0.50(5)	Irradiated 40 K[b]

[a]Broad component FWHM fixed.
[b]Warmed up to 100 K after irradiation.

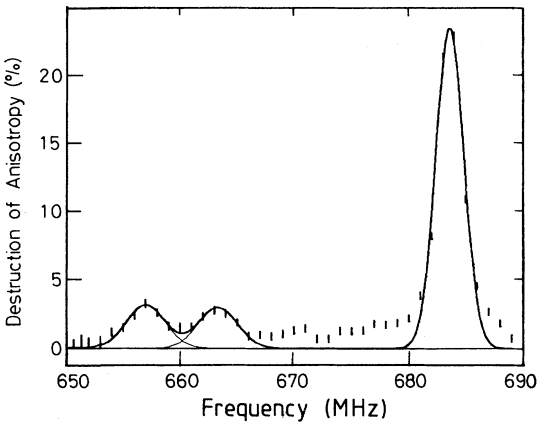

FIG. 8. NMRON spectrum for ⟨610⟩ crystal after irradiation with 5×10^{16} H^+/cm^2 at 225 K.

of the defect complex cannot be unambiguously inferred from this single measurement, the splitting of the resonance pattern into two lines with equal area suggests that the ⟨111⟩ symmetry is preserved. It should be noted that this defect was not observed after proton irradiation at low temperatures, probably because hydrogen associates with the stage-III defect which occurs before the latter becomes mobile. The hydrogen-decorated defects will have a reduced mobility. This may explain why defect trapping after proton irradiation and subsequent annealing at 240 K, as observed in Sec. IV A, is relatively inefficient.

In Sec. IV C it was reported that the stage-III defect could be produced quite well by irradiating the sample with He^+ above recovery-stage III. In this case the initial number of Frenkel pairs is roughly 16 times as large as for proton bombardment, and therefore it is likely that most He atoms get trapped at their own damage.

V. DISCUSSION

The picture of defect association that emerges from our results is rather limited, because we observed only one defect-associated site besides the substitutional site. After RT implantations we found $f_{NO}\approx0.5$, from which it is clear that a large fraction of the implanted atoms must have been in a low hyperfine field and contributes only weakly to the anisotropy at the temperatures that we used. The existence of such a field is in accordance with the Mössbauer results of de Waard *et al.*,[7] who studied ^{129}IFe formed by radioactive decay after RT implantation of ^{129m}Te into Fe. They found an additional hyperfine field of 46(4) T, which they tentatively assigned to an iodine-tetravacancy complex. Subsequent static nuclear orientation results of Rüter *et al.*,[18] obtained at temperatures down to 10 mK, yield the following site populations $f(B_{HF})$ for ^{131}I implanted into Fe at room temperature: $f(46\ T)=0.3$, $f(105\ T)=0.35$, and $f(115\ T)=0.35$. In order to explain our results in terms of these three sites, we must assume that about 50% of the iodine atoms is in the low-field site, which is rather unlikely. However, from the positron-annihilation results of Vehanen *et al.*, it is known that in electron-irradiated iron vacancies tend to form clusters of up to 10 atoms. In fact, the formation of impurity-multivacancy complexes was observed in many hyperfine interaction studies using the 5*sp* probes ^{111}In, ^{119}Sb, and ^{133}Xe (Refs. 22 and 23). It is likely, therefore, that iodine atoms will be found in different low-field sites.

The large value of f_{NO} observed after implantation at 20 K indicates that almost all iodine atoms must experience a hyperfine field close to 115 T. The tentative values for the site populations in Table V, however, do not add up to more than 0.6. In our view it is unlikely that this small value is the result of insufficient rf power only, because in that case the rf power would have to be increased by a factor of about 6 to approach saturation. We therefore suppose that there is an additional site for the implanted atoms, which gives rise to a hyperfine field close to 115 T. The corresponding resonance was not detected in our NMRON measurements and is probably outside the scanned frequency region from 610 to 690 MHz. Although the relative population of only two out of a number of sites could actually be determined, some definite conclusions can be reached, as will be discussed below.

A. Nature of the stage-III defect in α-Fe

The fact that the iodine-defect complex is formed in recovery-stage III, as shown in Secs. IV A–IV C, is in our opinion a sufficient proof that the defect involved in the formation of this complex and the stage-III defect are identical. We will now discuss the nature of this defect on the basis of our experimental results.

According to the two-interstitial model, metastable crowdions are mobile in stage I, while dumbbells move in stage III. The conversion from crowdions to dumbbells takes place either by thermal activation, or when the crowdion gets trapped at an impurity atom. The TIM predicts trapping of a dumbbell as a result of annealing following Frenkel pair production below stage III. One expects that the iodine-defect complex will be converted into another complex of interstitial type during postirradiation below stage III, and that the substitutional fraction will remain unchanged.[24]

The one-interstitial model predicts interstitial migration in stage I and vacancy migration in state III. It predicts that, after annealing following Frenkel pair production below stage III, vacancies are trapped. Also after implantation of a big impurity such as iodine, one expects trapping of one or more vacancies. However, after postirradiation below stage III, the substitutional fraction is predicted to increase at the expense of the vacancy-associated iodine atoms, through an antidefect reaction with mobile stage-I interstitials.

The decisive experiment to discriminate between the two models is the postirradiation below stage III (Sec. IV C), after which we observed a clear increase in the substitutional fraction. While predicted by the OIM, this result is in clear contradiction with the prediction of the TIM.

That we did not observe a decrease in the vacancy-associated fraction after postirradiation is readily explained by the presence of more complicated defects of vacancy type that were not detected with NMRON, as was discussed at the beginning of this section. Thus the total fraction of trapped monovacancies would be the net result of two competing processes: the production of monovacancies when multivacancy defects trap mobile interstitials and the simultaneous annihilation of monovacancies. This may quite well leave the total monovacancy fraction unchanged but will always increase the substitutional fraction. Apart from this argument, there are a number of other features that clearly favor the OIM.

(1) The prediction of the TIM that a dumbbell is trapped raises the question of what the symmetry of the resulting EFG will be. Although our interpretation of the spectra is somewhat biased by the assumption (in Sec. II) that the dipolar field is caused by a vacancy, it is clear that the quadrupole term gives the major contribution to the defect-associated hyperfine interaction. One therefore has to assume that there is an iodine-dumbbell complex that has a small asymmetry parameter η. Point-charge calculations of a dumbbell with a $\langle 110 \rangle$ orientation, which is the commonly accepted orientation for freely migrating dumbbells in α-Fe, show that the resulting EFG will have an asymmetry parameter which is substantially larger than the experimentally allowed maximum of 0.3. The only interstitial configuration that satisfies this requirement is, therefore, an interstitial defect with a $\langle 111 \rangle$ orientation. It is unlikely, however, that a dumbbell trapped at an oversized iodine atom would be oriented along a $\langle 111 \rangle$ axis, i.e., a close-packed direction.

(2) After low-temperature implantation (Sec. IV B) and after uncorrelated defect trapping (Sec. IV C), the same iodine-defect complex is formed. It is difficult to believe that for a big impurity such as iodine, dumbbells exclusively are trapped during low-temperature implantation.

(3) Following low-temperature implantation, the migration of interstitials at 130 K and the annihilation of the observed defect is clearly demonstrated through the accompanying narrowing of the substitutional line (Table IV). While perfectly natural for a vacancy-type defect complex, this is hard to explain on the basis of the TIM. We conclude that our results provide compelling evidence for the vacancy character of the defect that becomes mobile in α-Fe around 220 K (recovery-stage III).

B. The influence of vacancies on the site of implanted atoms

Comparing the results of the implantations at 20 K and at RT, we notice that in both cases monovacancies are trapped, but that f_{N0} is close to 1.0 after implantation at 20 K, whereas it is only 0.5 after implantation at RT. We conclude that monovacancies get trapped athermally in the collision cascade, probably as a result of replacement collisions. The lower substitutional fraction after implantation at RT is caused by thermal trapping of vacancies during the implantation process, resulting in multivacancy complexes that give rise to a low hyperfine field at the site of the iodine nucleus. It is also interesting to note that implantation at 20 K and subsequent annealing above stage III leads to a much higher high-field fraction than implantation at RT. This can be understood from the larger probability for recombination of Frenkel pairs in the former case.

These results agree quite well with the interpretation of Turos and Meyer,[25] whose channeling results on insoluble atoms implanted into Fe also show that a much higher substitutional fraction is attained after low-temperature implantation. Their conclusion, that vacancy trapping is the main factor that determines the lattice-site occupation of implanted atoms, is supported quite well by our results. It should be noted, however, that the rather low dose used in our low-temperature implantation, is probably a prerequisite to obtain such a high substitutional fraction.

VI. CONCLUSION

We can summarize the results of our NMRON measurements on ^{131}I as follows: The observed defect is of vacancy character and is very likely a monovacancy trapped by ^{131}I at a nearest-neighbor site. Lattice vacancies in α-Fe become mobile at about 220 K, in recovery-stage III. Implantation of a moderately low dose of iodine into iron at low temperature can lead to a large substitutional fraction, because in this case only athermal vacancy trapping takes place. RT implantation followed by light particle irradiation at a temperature between stages I_E and III leads to an increase of the substitutional fraction through defect-antidefect reactions.

ACKNOWLEDGMENTS

The authors are grateful to A. H. J. Timans for maintenance of the cryogenic equipment, F. Th. ten Broek for radiochemical assistance, J. J. Smit and E. H. van Voorthuysen for carrying out the implantations, L. Venema for preparation of the single crystals, and the staff of the van de Graaff accelerator for assistance during the irradiations. Special thanks are due to H. Schultz, Stuttgart, who kindly provided us with decarburized α-Fe single crystals. We also want to express our gratitude to K. Bethge, Frankfurt, who determined the impurity content of the samples. The assistance of F. Pleiter, who carefully read the manuscript, is kindly acknowledged. This work was performed as part of the research program of the Stichting voor Fundamenteel Onderzoek der Materie (FOM) with financial support from the Nederlandse Organisatie voor Wetenschappelijk Onderzoek (NWO).

[1]A. Vehanen, P. Hautojärvi, J. Johansson, J. Yli-Kauppila, and P. Moser, Phys Rev. B **25**, 762 (1982).

[2]A. Möslang, H. Graf, G. Balzer, E. Recknagel, A. Weidinger, Th. Wichert, and R. I. Grynszpan, Phys. Rev. B **27**, 2674 (1983).

[3]F. Phillipp, in *Proceedings of the International Conference on Vacancies and Interstitials in Metals and Alloys,* Vols. 15–18 of *Materials of Science Forum,* edited by C. Abromeit and H. Wollenberger (Trans Tech, Aedermannsdorf, 1987), p. 187.

[4]J. Wolf and H. Kronmüller, in *Proceedings of the International Conference on Vacancies and Interstitials in Metals and Alloys,* Ref. 3, p. 255.

[5]M. Hirscher, B. Schwendemann, W. Frank, and H. Kronmüller, in *Proceedings of the International Conference on Vacancies and Interstitials in Metals and Alloys,* Ref. 3, p. 249.

[6]S. Takaki, J. Fuss, H. Kugler, U. Dedek, and H. Schultz, Radiat. Effects **79**, 87 (1983).

[7]H. de Waard, R. L. Cohen, S. R. Reintsema, and S. A. Drentje, Phys. Rev. B **10**, 3760 (1974).

[8]F. Pleiter, C. Hohenemser, and A. R. Arends, Hyperfine Interact. **10**, 691 (1981).

[9]J. Golczewski, K. Maier, and W. Frank, Phys. Status Solidi B **134**, 551 (1986).

[10]*Low Temperature Nuclear Orientation,* edited by N. J. Stone and H. Postma (Elsevier Science, Amsterdam, 1986).

[11]D. Visser, L. Niesen, H. Postma, and H. de Waard, Phys. Rev. Lett. **41**, 882 (1978).

[12]A. Metz, in *Nuclear Physics Applications to Materials Science,* edited by E. Recknagel and J. C. Soares (Kluwer, Dordrecht, 1988), p. 435.

[13]*Table of Isotopes,* 7th ed., edited by C. M. Lederer and V. S. Shirley (Wiley, New York, 1978).

[14]E. Matthias, W. Schneider, and R. M. Steffen, Arkif Fysik **24**, 97 (1963).

[15]B. K. S. Koene and H. Postma, Nucl. Phys. **A219**, 563 (1974).

[16]E. Hagn, K. Leuthold, E. Zech, and H. Ernst, Z. Phys. **A295**, 385 (1980).

[17]P. Jung, J. Nucl. Mater. **117**, 70 (1983).

[18]H. D. Rüter, W. Haaks, E. W. Duczynski, E. Gerdau, D. Visser, and L. Niesen, Hyperfine Interact. **9**, 385 (1981).

[19]D. Visser, Ph.D. thesis, Groningen, 1981.

[20]O. Meyer and A. Turos, Nucl. Instrum. Methods **B19/20**, 136 (1987).

[21]J. Vökl and G. Alefeld, in *Diffusion in Solids, Recent Developments,* edited by A. S. Nowick and J. J. Burton (Academic, New York, 1975), p. 252. The authors give two data sets for hydrogen in Fe, from which we chose the data predicting the slowest diffusion.

[22]E. Recknagel, G. Schatz, and Th. Wichert, in *Hyperfine Interactions of Radioactive Nuclei,* Vol. 31 of *Topics in Current Physics,* edited by J. Christiansen (Springer, Berlin, 1983), p. 133.

[23]H. de Waard and L. Niesen, in *Mössbauer Spectroscopy Applied to Inorganic Chemistry,* edited by G. J. Long (Plenum, New York, 1987), p. 1.

[24]J. Golczewski and W. Frank, Phys. Status Solidi B **138**, 123 (1986).

[25]O. Meyer and A. Turos, Mater. Sci. Rep. **2**, 373 (1987).